

Quantum stochastic resonance in an a.c.-driven single-electron quantum dot

Timo Wagner^{1*}, Peter Talkner², Johannes C. Bayer¹, Eddy P. Rugeramigabo¹, Peter Hänggi^{2,3} and Rolf J. Haug¹

In stochastic resonance, the combination of a weak signal with noise leads to its amplification and optimization¹. This phenomenon has been observed in several systems in contexts ranging from palaeoclimatology, biology, medicine, sociology and economics to physics^{1–9}. In all these cases, the systems were either operating in the presence of thermal noise or were exposed to external classical noise sources. For quantum-mechanical systems, it has been theoretically predicted that intrinsic fluctuations lead to stochastic resonance as well, a phenomenon referred to as quantum stochastic resonance^{1,10,11}, but this has not been reported experimentally so far. Here we demonstrate tunnelling-controlled quantum stochastic resonance in the a.c.-driven charging and discharging of single electrons on a quantum dot. By analysing the counting statistics^{12–16}, we demonstrate that synchronization between the sequential tunnelling processes and a periodic driving signal passes through an optimum, irrespective of whether the external frequency or the internal tunnel coupling is tuned.

Stochastic resonance is known to arise in noisy bistable systems with proper periodic modulation of the switching rates. It manifests itself as an optimal synchronization of the driving signal with the switching process, as a function of the driving frequency f as well as the noise level. As a rule of thumb, this optimum occurs at^{1,13}

$$2f \approx \Gamma_S \quad (1)$$

when the doubled driving frequency $2f$ approximately corresponds to the unperturbed switching rate Γ_S . The switching rate Γ_S thereby characterizes the noise spectrum of the system. Because stochastic resonance does not depend on the concrete physical realization of the system, this timescale matching condition should also be applicable to the tunnelling process between two quantum states. The noise source in that case is the intrinsic shot noise, which stems directly from the random quantum mechanical tunnelling dynamics. To observe stochastic resonance in an a.c.-driven quantum dot, one needs to precisely control the tunnelling process between two quantum states of the quantum dot and measure the temporal fluctuations.

Figure 1a presents a scanning electron microscopy (SEM) image of our device structure as well as a schematic of the experimental set-up. The quantum dot (green e^- island) is formed electrostatically by nanosized gate electrodes and behaves physically like an artificial atom, which can be charged or discharged via two tunnel-coupled electron reservoirs¹⁷. This single-electron charging process is sensed directly with the capacitively coupled quantum point contact (QPC), operated as a time-resolved charge detector^{15,16}. The number N_e of

bound electrons on the quantum dot is set in a controlled manner via the three gate voltages $V_G = (V_{d1}, V_{d2}, V_{d3})$. Figure 1b presents a gate-dependent charge stability diagram of the quantum dot in the few-electron regime. Along the visible charging lines, a quantum dot charge state μ_N is energetically close to the Fermi level μ_F of the tunnel-coupled reservoirs, allowing electrons to tunnel back and forth between the quantum dot and the reservoirs. The thermal energy $k_B T = 130 \mu\text{eV}$ at $T = 1.5 \text{ K}$ is much smaller than the charging energy $E_c \approx 2.5 \text{ meV}$. E_c is the difference between the electrochemical potential of the N th and $(N-1)$ st electron. Therefore, only one additional electron can occupy the quantum dot at any given time (Coulomb blockade), causing sequential ‘in’ and ‘out’ tunnelling.

We set our experimental operation point V_{OP} at the first charging line, indicated as $N_e = 1$ in Fig. 1b, where the electron number on the quantum dot fluctuates between zero and one. For the driving we periodically modulated the three gate voltages

$$V_G(t) = V_{OP} + \mathbf{e}_d A \sin(2\pi f t) \quad (2)$$

with frequency f , amplitude A and in the direction of the unit vector \mathbf{e}_d .

To study the synchronization between the deterministic external a.c. drive and internal stochastic tunnelling process, the detector current $I_{qpc}(t)$ was monitored. A short snapshot of a typical detector trace is displayed in Fig. 1c, which directly reveals the sequential charging and discharging of the quantum dot. Whenever an electron tunnels into the quantum dot the current I_{qpc} jumps down, and it jumps up again when the electron tunnels out. From the detector traces we extract the times $t_{in,out}$ of all ‘in’ and ‘out’ tunnelling events (Fig. 1d).

The fluctuations in the occupation are characterized by the single-electron counting statistics¹⁴. We thus counted the total number $n(T_f)$ of ‘in’ and ‘out’ tunnelling events within one driving period T_f . From all possible periods and phases of the a.c. drive we finally obtained a counting probability $P(n)$ (Fig. 1e). A quantitative measure for the fluctuations is given by the Fano factor

$$F = \frac{\sigma^2}{\langle n \rangle} = \frac{\langle n^2 \rangle - \langle n \rangle^2}{\langle n \rangle} \quad (3)$$

calculated from the variance $\sigma^2 = \langle n^2 \rangle - \langle n \rangle^2$ and the mean $\langle n \rangle$ of the counting probability $P(n)$. For a strictly Poissonian random process the Fano factor equals $F = 1$. Without external a.c. drive the Fano factor always exceeds or equals this Poissonian limit (that is, $F \geq 1$) due to the bunching of tunnelling-in and tunnelling-out

¹Institut für Festkörperphysik, Leibniz Universität Hannover, Hannover, Germany. ²Institut für Physik, Universität Augsburg, Augsburg, Germany.

³Nanosystems Initiative Munich, Munich, Germany. *e-mail: wagner@nano.uni-hannover.de

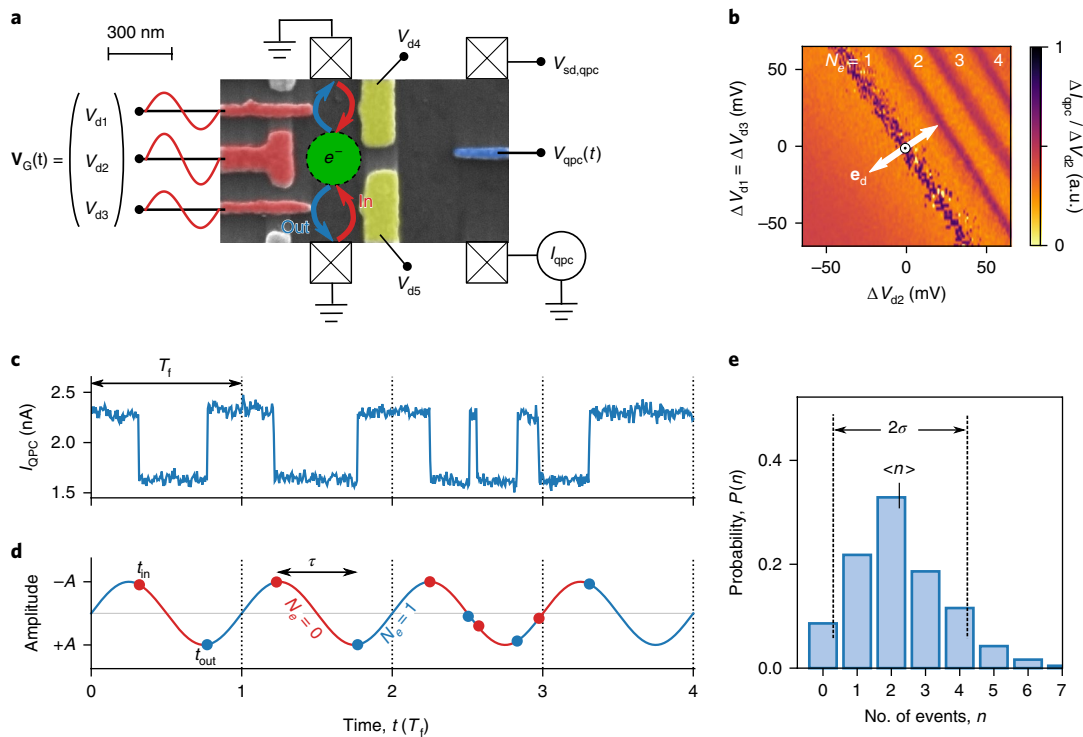


Fig. 1 | Experimental set-up, device operation and statistical analysis. **a**, SEM image of the device structure with a schematic of the experimental set-up. The quantum dot (green e^- island) is defined electrostatically by the red gates $V_{d1,d2,d3}$ and yellow gates $V_{d4,d5}$. The QPC charge detector is formed by the blue gate V_{qpc} . The quantum dot and QPC current paths are galvanically isolated from each other; the visible gap between the yellow middle gates is closed electrostatically and has the purpose of enhancing detector sensitivity. The quantum dot can be charged and discharged by electrons tunnelling in from (red arrow) and tunnelling out to (blue arrow) the coupled electron reservoirs. The tunnelling process is controlled and driven periodically by the three gate voltages $V_G = (V_{d1}, V_{d2}, V_{d3})$. Crossed squares indicate the ohmic contacts of the sample. **b**, Charge stability diagram of the quantum dot in the few-electron regime. The operation point $V_{G,OP}$ is indicated by a circle with a dot at the charging line $N_e = 1$. The gate voltages V_G are periodically modulated along the highlighted direction e_d . **c**, A typical time-resolved current trace $I_{QPC}(t)$ of the QPC charge detector, revealing the sequential charging and discharging of the quantum dot. The shown trace was recorded with a drive of $f = 800$ Hz and an amplitude of $A = 10$ mV. **d**, Extracted ‘in’ (red) and ‘out’ (blue) tunnelling events relative to the external a.c. drive. The times t_{in}, t_{out} and the residence times τ are extracted from the detected events. **e**, Counting statistics $P(n)$ for the number of tunnelling events within one driving period T_f . The Fano factor $F = \sigma^2 / \langle n \rangle$, equation (3), of the distribution is calculated from the mean $\langle n \rangle$ and variance $\sigma^2 = \langle n^2 \rangle - \langle n \rangle^2$ of the distribution.

events (Supplementary Fig. 1). The driving-dependent antibunching of tunnelling events, signalled by a suppression of the Fano factor below the Poissonian limit (that is, $F < 1$) thus provides an unambiguous measure of the synchronization strength¹⁴.

The red circles in Fig. 2 depict the experimentally determined Fano factor F as a function of external driving frequency f . Additionally, the inset shows the corresponding mean counts $\langle n \rangle$ per period. The amplitude $A = 10$ mV was kept constant for all frequencies. The experimental Fano factor F has a minimum at $f = 800$ Hz, providing evidence for stochastic resonance. At the minimum, essentially two tunnelling events (one ‘in’ and one ‘out’) occur on average per driving period ($\langle n \rangle \approx 2$), corroborating the optimal synchronization between external a.c. drive and internal tunnelling. If the a.c. drive is too slow ($f \ll 800$ Hz), more than two tunnelling events occur within one period ($\langle n \rangle \gg 2$) and the Fano factor F increases above the Poissonian limit. If the drive is instead too fast ($f \gg 800$ Hz), most electrons need multiple periods to tunnel in and out of the quantum dot ($\langle n \rangle \ll 2$) and the Fano factor F approaches the Poissonian limit from below.

Because the ‘in’ and the ‘out’ tunnelling events are alternating, and hence their occurrences are strictly dependent, stochastic resonance can be equally characterized on the basis of the occurrences of the specific tunnel events (Supplementary Fig. 2) or on the basis of the set of all transitions independent of their direction, as we do here. To demonstrate, in the presently investigated system, that the

general mechanisms of stochastic resonance are at play, we extracted the tunnelling rates $\Gamma_{in}(t)$ and $\Gamma_{out}(t)$ with which an electron enters and leaves the quantum dot at time t , respectively, from the experimental data (see Methods).

Figure 3a displays the tunnelling-in and tunnelling-out rates for a quantum dot with driving frequency $f = 800$ Hz and amplitude $A = 10$ mV in the direction e_d , as indicated in Fig. 1b. The in rate (red) instantly follows the external a.c. driving voltage, as given by equation (2), without any visible delay, corroborated by the fact that the rate at half of the period agrees with its initial value, $\Gamma_{in}(0) = \Gamma_{in}(T_f/2)$. The out rate (blue) is shifted by a half period $T_f/2$ relative to the in rate and also agrees at half of the period with its initial value, $\Gamma_{out}(0) = \Gamma_{out}(T_f/2)$. This asymmetric modulation of the rates is caused by the periodic shift of the charging state $\mu_0(t)$ around the symmetry level μ_s , as illustrated in Fig. 3b. At the symmetry level $\mu_s = \mu_0(t = 0, \frac{1}{2}T_f, T_f, \dots)$ the in and out rates are equal. In the first half of a period ($0 < t < T_f/2$) the charging state is pushed below the symmetry level, that is $\mu_0 < \mu_s$, causing an enhancement of the in rate and a suppression of the out rate. An electron tunnels from the reservoir most probably into the quantum dot when the charge state is at its energetically lowest position ($t = \frac{1}{4}T_f, \frac{5}{4}T_f, \dots$). In the second half of a period ($T_f/2 < t < T_f$) the charging state is instead pushed above the symmetry level,

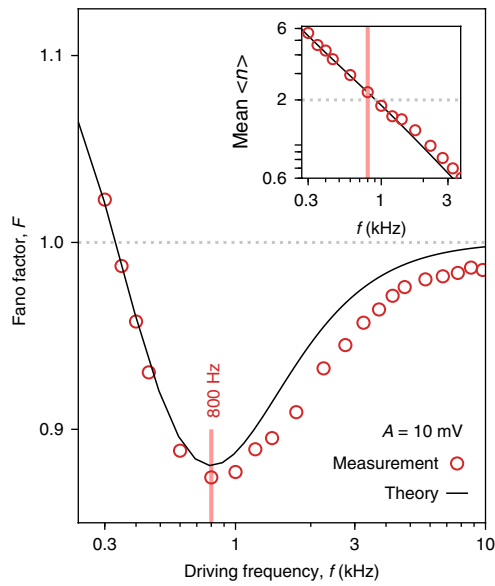


Fig. 2 | Frequency-dependent stochastic resonance. Experimental (red circles) and theoretical (black line) Fano factor F as a function of driving frequency f . The experimental data have a minimum at $f=800$ Hz, in good agreement with the theoretical resonance frequency. Inset, Corresponding average number of tunnelling events per period $\langle n \rangle$. At the resonance frequency (vertical red line) nearly two tunnelling events ($\langle n \rangle \approx 2$) occur on average per period.

that is $\mu_0 > \mu_s$. There, the in rate is suppressed and the out rate is enhanced. The best opportunity to tunnel out occurs at the energetically highest position ($t = \frac{3}{4}T_f, \frac{7}{4}T_f, \dots$). The transition rates $\Gamma_{in}(t)$ and $\Gamma_{out}(t)$ specify a two-state Markovian process for which the counting probability $P(n)$ can be determined^{13,14} (see Methods). The theoretical results for the first moment of the number of transitions and the Fano factor are in good agreement with the respective direct experimental outcomes, as can be seen from Figs. 2 and 4.

The resonance frequency $f=800$ Hz at which the Fano factor attains its minimum also conforms well with the stochastic rule

of thumb. The double resonance frequency $2f \approx 1,600$ Hz approximately matches the tunnel coupling $\Gamma_s \approx 1,675$ Hz at the symmetry level μ_s . When the driving frequency is much faster than the tunnel coupling (that is, $\Gamma_s \ll 2f$, an electron easily ‘misses’ the first good opportunity to tunnel and will wait until another good opportunity occurs, one or several periods later. These findings show that the variation of the frequency f conforms well with the idea of stochastic resonance as a resonance phenomenon.

The so-called ‘residence time’ is given by the time span during which a quantum dot is occupied without interruption¹. As a random variable it is characterized by a probability density function (p.d.f.), denoted as $\rho_1(\tau)$. The blue dots in Fig. 3c display the experimentally determined residence time p.d.f. The residence time p.d.f. for fast driving with $f=10$ kHz consists of a train of maxima at odd integer multiples of the half period¹, that is $\tau_k = (2k+1)T_f/2$, $k=0,1,2,\dots$, demonstrating the waiting of the electron for a good tunnelling opportunity. At the resonance frequency $f=800$ Hz instead, obeying $2f \approx \Gamma_s$, $\rho_1(\tau)$ quickly decreases with increasing residence times with a strong shoulder at $T_f/2$ and a weak shoulder at $3T_f/2$, indicating optimal synchronization between internal tunnelling and the external a.c. drive.

Under the assumption that the time-periodic rates $\Gamma_{in/out}(t)$ govern a Markovian process of alternate visits of the occupied (1) and empty (0) quantum dot states, the residence time p.d.f., $\rho_1(\tau)$, can be calculated¹⁴ (see Methods). Figure 3c demonstrates that the residence time p.d.f.s from the Markovian model (solid lines) agree nicely with experimental statistics.

So far, we have succeeded in showing that the synchronization can be optimized by tuning the driving frequency f . Alternatively, one may aim at synchronizing a signal at fixed frequency f . Thereby, the tunnel coupling Γ_s needs to be adapted to the double driving frequency $2f$. The coupling Γ_s depends on the size of the tunnel barriers, as illustrated in Fig. 4a. We tuned the coupling by shifting the operation point $V_{G,OP}$ along the charging line (Fig. 1b). The driving frequency $f=1$ kHz and the amplitude $A=10$ mV were kept constant. The experimentally determined Fano factor F is plotted as a function of the tunnel coupling Γ_s in Fig. 4b and the inset shows the corresponding mean $\langle n \rangle$ of the counting statistics. The experimental Fano factor F has a minimum at 1.75 kHz, which is close to the double driving frequency $2f=2$ kHz. At the minimum we also find nearly two tunnelling events per period

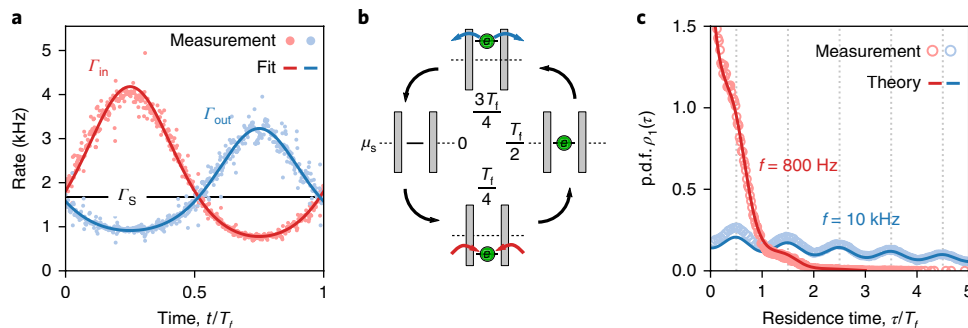


Fig. 3 | Temporal modulation of the tunnelling process. **a**, Experimentally time-dependent tunnelling-in rate $\Gamma_{in}(t)$ (red dots) and tunnelling-out rate $\Gamma_{out}(t)$ (blue dots). The rates were extracted for a drive with $f=800$ Hz and $A=10$ mV. The fits (solid lines) are based on a Fourier expansion of the logarithm of the rates. The horizontal black line marks the tunnel coupling $\Gamma_s=1,675$ Hz at symmetry level μ_s . **b**, Asymmetric modulation of the rates is caused by the periodic shift of the quantum dot charging state around the symmetry level μ_s . At the symmetry level μ_s ($t=0, T_f/2$), the two tunnelling rates are identical. An electron tunnels from reservoirs most probably into the quantum dot when the charge state is at its lowest position ($t=T_f/4$). The best opportunity to tunnel out of the quantum dot occurs when the charging state reaches its energetically highest position ($t=3T_f/4$). **c**, Periodic modulation of the tunnelling process is also observable in the residence time probability density $\rho_1(\tau)$. For a fast driving frequency $f=10$ kHz, the residence time probability density function (p.d.f.) $\rho_1(\Delta t)$ displays a train of maxima at odd integer multiples of the half period $\tau_k = (2k+1)T_f/2$, $k=0,1,2,\dots$. At the lower driving frequency $f=800$ Hz, the maximum at $T_f/2$ is accompanied by considerably suppressed satellites. In both cases the agreement between experiment (dots) and theory (solid lines) is striking.

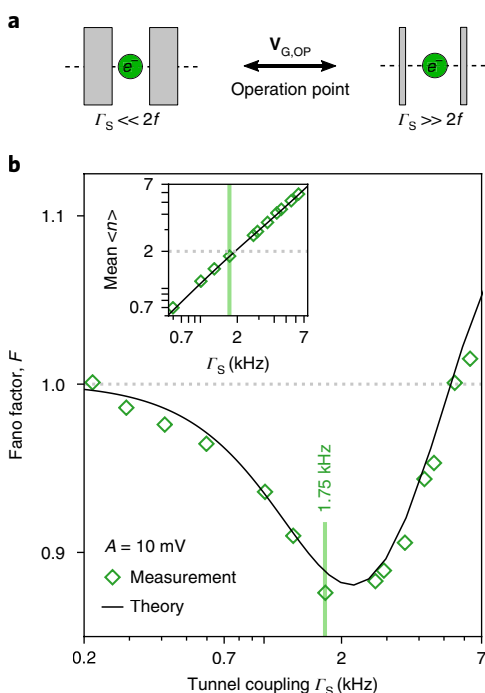


Fig. 4 | Tunnel coupling-dependent stochastic resonance. **a**, The tunnel coupling Γ_S of the quantum dot depends on the size of the tunnel barriers, which can be altered by choosing a different operation point $V_{G,OP}$ on the first charging line. This way, the tunnel coupling can be tuned from values smaller than to values much larger than the double driving frequency $2f$. **b**, Experimental (green diamonds) and theoretical (black line) Fano factor F as a function of tunnel coupling Γ_S . The experimental data have a minimum at $\Gamma_S = 1.75$ kHz, in good agreement with the minimum of the theoretical model. The driving parameters were $f = 1$ kHz and $A = 10$ mV. Inset, Corresponding average number of tunnelling events per period $\langle n \rangle$ as a function of tunnel coupling. At the resonance frequency (vertical green line) nearly two tunnelling events (for example, $\langle n \rangle \approx 2$; one 'in' and one 'out') occur on average per period.

($\langle n \rangle \approx 2$), corroborating the optimal synchronization of the Rice frequency defined as the rate of transition events into the occupied state^{12,13}. Furthermore, we compared the experimental results with the outcome of the Markovian two-state model. According to our empirical finding the rates at different operation points are proportional to the tunnel coupling Γ_S . Therefore, the rates are given by $\Gamma_{in/out}(t, \Gamma_S) = (\Gamma_S / \Gamma_S^*) \Gamma_{in/out}^*(t, \Gamma_S^*)$. As reference we chose the extracted tunnelling rates (see Methods) with $\Gamma_S^* = 1,675$ Hz. Figure 4 displays good agreement between the resulting theoretical Fano-factors and the average numbers of transitions with the according experimental findings.

We emphasize that there is a crucial difference between the variation of the external driving frequency f and the internal tunnel coupling Γ_S . With a change of frequency f , the time averages of the transition rates as well as the values of their minima and maxima remain the same, while both rate characteristics alter upon a variation of the tunnel coupling Γ_S . Hence the variation of Γ_S corresponds more closely to the original characterization of the stochastic resonance phenomena, indicating that an increase of the noise up to a certain level can lead, counter-intuitively, to an improved signal-to-noise ratio.

Such a.c.-driven single-electron tunnelling has also been studied intensively in the form of turnstiles¹⁸, ratchets¹⁹ and pumps²⁰, the latter being promising candidates for the redefinition of the ampere²¹. The functionality of these devices is based on the locking of the mean

counts $\langle n \rangle = \text{const.}$, meaning that the number of transferred electrons per period is frequency independent and robust against noise. For the stochastic resonance discussed here with a relatively weak driving amplitude $A = 10$ mV, locking is not present, as is evident from the inset of Fig. 2. The observed synchronization is a consequence of the timescale matching of the external a.c. drive and the internal tunnelling process. At a larger amplitude, $A = 30$ mV (Supplementary Fig. 3), however, the average number of transitions starts to develop plateaux around the respective resonance values of frequency and tunnel coefficient, in accordance with theoretical^{12–14} and experimental²² observations for strongly a.c.-driven stochastic resonance systems. This confirms that the locking in a.c.-driven single-electron devices is subject to the same statistical physics and can be seen as a special case of stochastic resonance in the limit of strong a.c. driving.

Stochastic resonance in a.c.-driven single-electron tunnelling should also occur in direct shot-noise measurements²³ or corresponding heat and work distributions²⁴. The optimal working point for on-demand single-electron sources^{25,26}, which provide an important toolbox for quantum electronics, is defined by tunnelling-driven stochastic resonance. Quantum dots have been utilized successfully as displacement sensors for nanomechanical oscillators^{27,28}. Their resolution is thought to be limited by the standard quantum limit, due to the stochastic backaction of the single-electron tunnelling process. The phenomenon of tunnelling-driven stochastic resonance provides a way to overcome this limit.

Online content

Any methods, additional references, Nature Research reporting summaries, source data, statements of data availability and associated accession codes are available at <https://doi.org/10.1038/s41567-018-0412-5>.

Received: 6 September 2017; Accepted: 20 December 2018; Published online: 4 February 2019

References

- Gammaitoni, L., Hänggi, P., Jung, P. & Marchesoni, F. Stochastic resonance. *Rev. Mod. Phys.* **70**, 223–288 (1998).
- Lee, I. Y., Liu, X. L., Kosko, B. & Zhou, C. W. Nanosignal processing: stochastic resonance in carbon nanotubes that detect subthreshold signals. *Nano Lett.* **3**, 1683–1686 (2003).
- Badzey, R. L. & Mohanty, P. Coherent signal amplification in bistable nanomechanical oscillators by stochastic resonance. *Nature* **437**, 995–998 (2005).
- Nishiguchi, K. & Fujiwara, A. Detecting signals buried in noise via nanowire transistors using stochastic resonance. *Appl. Phys. Lett.* **101**, 193108 (2012).
- Venstra, W. J., Westra, H. J. R. & van der Zant, H. S. J. Stochastic switching of cantilever motion. *Nat. Commun.* **4**, 2624 (2013).
- Abbaspour, H., Trebaol, S., Morier-Genoud, F., Portella-Oberli, M. T. & Deveaud, B. Stochastic resonance in collective exciton-polariton excitations inside a GaAs microcavity. *Phys. Rev. Lett.* **113**, 057401 (2014).
- Sun, G. et al. Detection of small single-cycle signals by stochastic resonance using a bistable superconducting quantum interference devices. *Appl. Phys. Lett.* **106**, 172602 (2015).
- Stroescu, I., Hume, D. B. & Oberthaler, M. K. Dissipative double-well potential for cold atoms: kramers rate and stochastic resonance. *Phys. Rev. Lett.* **117**, 243005 (2016).
- Monifi, F. et al. Optomechanically induced stochastic resonance and chaos transfer between optical fields. *Nat. Photon.* **10**, 399–405 (2016).
- Löfstedt, R. & Coppersmith, S. N. Quantum stochastic resonance. *Phys. Rev. Lett.* **72**, 1947–1950 (1994).
- Grifoni, M. & Hänggi, P. Coherent and incoherent quantum stochastic resonance. *Phys. Rev. Lett.* **76**, 1611–1614 (1996).
- Callenbach, L., Hänggi, P., Linz, S. J., Freund, J. A. & Schimansky-Geier, L. Oscillatory systems driven by noise: frequency and phase synchronization. *Phys. Rev. E* **65**, 051110 (2002).
- Talkner, P. Statistics of entrance times. *Physica A* **325**, 124–135 (2003).
- Talkner, P., Machura, L., Schindler, M., Hänggi, P. & Luczka, J. Statistics of transition times, phase diffusion and synchronization in periodically driven bistable systems. *New J. Phys.* **7**, 14 (2005).
- Gustavsson, S. et al. Counting statistics of single-electron transport in a quantum dot. *Phys. Rev. Lett.* **96**, 076605 (2006).

16. Wagner, T. et al. Strong suppression of shot noise in a feedback-controlled single-electron transistor. *Nat. Nanotechnol.* **12**, 218–222 (2017).
17. Kouwenhoven, L. P., Austing, D. G. & Tarucha, S. Few-electron quantum dots. *Rep. Prog. Phys.* **64**, 701–736 (2001).
18. Kouwenhoven, L. P., Johnson, A. T., van der Vaart, N. C., Harmans, C. J. P. M. & Foxon, C. T. Quantized current in a quantum-dot turnstile using oscillating tunnel barriers. *Phys. Rev. Lett.* **67**, 1626–1629 (1991).
19. Platonov, S. et al. Lissajous rocking ratchet: realization in a semiconductor quantum dot. *Phys. Rev. Lett.* **115**, 106801 (2015).
20. Blumenthal, M. D. et al. Gigahertz quantized charge pumping. *Nat. Phys.* **3**, 343–347 (2007).
21. Pekola, J. P. et al. Single-electron current sources: toward a refined definition of the ampere. *Rev. Mod. Phys.* **85**, 1421–1472 (2013).
22. Shulgin, B., Neiman, A. & Anishchenko, V. Mean switching frequency locking in stochastic bistable systems driven by a periodic force. *Phys. Rev. Lett.* **75**, 4157–4160 (1995).
23. Burk, H., de Jong, M. J. M. & Schönberger, C. Shot-noise in the single-electron regime. *Phys. Rev. Lett.* **75**, 1610–1613 (1995).
24. Pekola, J. P. Towards quantum thermodynamics in electronic circuits. *Nat. Phys.* **11**, 118–123 (2015).
25. Fève, G. et al. An on-demand coherent single-electron source. *Science* **316**, 1169–1172 (2007).
26. Albert, M., Flindt, C. & Büttiker, M. Distributions of waiting times of dynamic single-electron emitters. *Phys. Rev. Lett.* **107**, 086805 (2011).
27. Mozyrsky, D., Martin, I. & Hastings, M. B. Quantum-limited sensitivity of single-electron-transistor-based displacement detectors. *Phys. Rev. Lett.* **92**, 018303 (2004).
28. LaHaye, M. D., Buu, O., Camarota, B. & Schwab, K. C. Approaching the quantum limit of a nanomechanical resonator. *Science* **304**, 74–77 (2004).

Acknowledgements

This work was supported financially by the Research Training Group 1991 (DFG), the School for Contacts in Nanosystems (NTH), the Center for Quantum Engineering and Space-Time Research (QUEST), the Laboratory for Nano and Quantum Engineering (LNQE) and the ‘Fundamentals of Physics and Metrology’ initiative (T.W., J.C.B., E.R. and R.J.H.).

Author contributions

T.W. carried out the experiments, analysed the data and wrote the manuscript. J.C.B. and T.W. fabricated the device. E.P.R. grew the wafer material. P.T. and P.H. provided theory support. T.W., P.T., P.H. and R.J.H. discussed the results. R.J.H. supervised the research. All authors contributed to editing the manuscript.

Competing interests

The authors declare no competing interests.

Additional information

Supplementary information is available for this paper at <https://doi.org/10.1038/s41567-018-0412-5>.

Reprints and permissions information is available at www.nature.com/reprints.

Correspondence and requests for materials should be addressed to T.W.

Journal peer review information: *Nature Physics* thanks Christian Flindt and the other anonymous reviewers for their contribution to the peer review of this work.

Publisher’s note: Springer Nature remains neutral with regard to jurisdictional claims in published maps and institutional affiliations.

© The Author(s), under exclusive licence to Springer Nature Limited 2019

Methods

Experimental set-up. Our quantum dot device is based on a GaAs/AlGaAs heterostructure, which forms a two-dimensional electron gas (2DEG) 100 nm below the surface. The 2DEG charge carrier density is $n_e = 2.4 \times 10^{11} \text{ cm}^{-2}$, and the mobility is $\mu_e = 5.1 \times 10^5 \text{ cm}^2 \text{ V}^{-1} \text{ s}^{-1}$. On the surface we patterned nanosized metallic top gates (7 nm Cr, 30 nm Au) using electron-beam and optical lithography. The quantum dot and QPC are formed electrostatically. By applying negative voltages to the gates, we deplete the 2DEG below.

All measurements were carried out on a low-noise d.c. transport set-up in a ⁴He cryostat at 1.5 K. Filtering and signal amplification were fully carried out outside the cryostat at room temperature. All gates were filtered by a 1 MHz low-pass filter. The QPC source was filtered by a 10 Hz low-pass filter and a 1:1,000 voltage divider was used to increase the resolution. The QPC charge detector current was amplified with a low-noise FEMTO transimpedance amplifier (100 MV A⁻¹ gain, 100 kHz bandwidth), connected to the QPC drain by a 25 pF low-capacity coaxial line. An Adwin Pro2 real-time system was used (1 GHz ADSP T12) to supply the voltage (16-bit digital-to-analog convertor card) and to record the QPC detector signal (18-bit analog-to-digital convertor card) for the statistical analysis. The a.c. signals were also generated by the ADwin system. The input and output sampling rates were $\Gamma_s = 400 \text{ kHz}$.

To minimize the crosstalk with the drive, the detector was kept at a constant working point by periodically adjusting the QPC gate voltage $V_{\text{qpc}}(t)$.

The detector current $I_{\text{qpc}}(t)$ was monitored with a temporal resolution of $\Delta t_s = 2.5 \mu\text{s}$. For significant statistics we always recorded traces for a duration of 10 min, typically extended over 10^5 – 10^7 driving periods and containing approximately 10^6 tunnelling events.

Extraction of tunnelling rates. Starting from a long detector trace of alternating in and out states the numbers $N_{\text{in}}(t_e)$ ($N_{\text{out}}(t_e)$) with which an electron has entered (left) the quantum dot within a bin of width Δt_s around $t_e = t \bmod T_f$ and the numbers $N_0(t_e)$ ($N_1(t_e)$) representing how often the quantum dot is empty (occupied) within the same bin are determined. On the basis of these numbers one can estimate the conditional probabilities of a transition to the occupied state within the interval Δt_s as $p(1, t + \Delta t_s | 0, t) = N_{\text{in}}(t_e) / N_0(t_e)$ and, similarly, of a transition to an empty dot as $p(0, t + \Delta t_s | 1, t) = N_{\text{out}}(t_e) / N_1(t_e)$. For a sufficiently small bin width Δt_s , the conditional probabilities can be expanded as $p(1, t + \Delta t_s | 0) \approx \Gamma_{\text{in}}(t) \Delta t_s$ and $p(0, t + \Delta t_s | 1) \approx \Gamma_{\text{out}}(t) \Delta t_s$, yielding for the time-periodically varying rates

$$\begin{aligned} \Gamma_{\text{in}}(t) &= \frac{1}{\Delta t_s} \frac{N_{\text{in}}(t_e)}{N_0(t_e)} \\ \Gamma_{\text{out}}(t) &= \frac{1}{\Delta t_s} \frac{N_{\text{out}}(t_e)}{N_1(t_e)} \end{aligned} \quad (4)$$

The dots in Fig. 3a represent the results of equation (4) for bin width $\Delta t_s = T_f/500$. Solid lines are fits based on a Fourier expansion of the logarithm of the rate with at most three higher harmonics. The experimental in and out rates do not cross exactly at $t = 0, T_f/2, \dots$, because the charging state was not perfectly adjusted to the symmetry level μ_s . Also, the experimental rates differ slightly in their form. This has two main causes. First, the two tunnelling processes are differently affected due the twofold spin degeneracy of the first charging state^{29,30}, which slightly shifts the symmetry level $\mu_s = \mu_F + k_B T / \sqrt{2}$ above the Fermi level μ_F . Second, the a.c. drive also modulates the size of the tunnelling barriers.

Generally, the in and out rates exhibit a non-trivial dependence on the driving frequency f . Because, in the present case, the driving frequency f is much smaller than any electronic or phononic timescale relevant for the tunnelling process of an

electron, the rates depend adiabatically on the frequency f , that is $\Gamma_{\text{in/out}}(t, f) = \Gamma_{\text{in/out}}(t/f, f)$, where f is a reference frequency, which we chose as $f = 800 \text{ Hz}$.

Counting statistics. For the two-state Markov process with periodically time-dependent rates $\Gamma_{\text{in}}(t)$ and $\Gamma_{\text{out}}(t)$, the probabilities $p_\alpha(n; t, s)$ to find the quantum dot at time s in the empty or the occupied state $\alpha = 0, 1$, respectively, and to observe n transitions until the time $t > s$ can be calculated as the solution of a hierarchy of first-order differential equations with respect to time t (refs. ^{13,14}). This hierarchy can be solved successively starting at $n = 0$. Choosing in $p_\alpha(n; t, s)$ the later time as $t = T_f + s$ with $0 \leq s < T_f$ one obtains the counting statistics $P(n; s) = p_0(n, T_f + s, s) + p_1(n, T_f + s, s)$ for the number of transitions within a period, which still depend on the initial phase $2\pi s / T_f$ at which the counting window begins. For a comparison with the experimental, phase-averaged results the mean over this phase is performed, yielding the averaged counting statistics $P(n) = \int_0^{T_f} ds P(n; s) / T_f$, from which the moments of n and the Fano factor can be determined. The theoretical results for the first moment of the number of transitions and the Fano factor are in good agreement with the respective direct experimental outcomes, as can be seen from Figs. 2 and 4. The average number of transitions per period at the minimum is only slightly larger than two, in accordance with the matching condition of the driving frequency with the average Rice frequency defined as the rate of transition events into the occupied state^{12,13}.

Residence time p.d.f. The residence time p.d.f. $\rho_1(\tau)$ can be obtained in terms of the conditional p.d.f. $\rho(\tau|s) = \Gamma_{\text{out}}(\tau + s) P_1(\tau + s | s)$ to find the quantum dot occupied without interruption during the time span $(s, s + \tau)$, where $P_1(\tau + s | s) = \exp\left\{-\int_s^{\tau+s} dt \Gamma_{\text{out}}(t)\right\}$ denotes the probability for a quantum dot being permanently occupied from s to $\tau + s$. To obtain the residence time p.d.f. the conditional p.d.f. $\rho_1(\tau|s)$ must be averaged with respect to the time s at which an electron occupies the quantum dot. These events occur according to the p.d.f. $\rho_{\text{in}}(s) = \Gamma_{\text{in}}(s) p_0(s) / \int_0^{T_f} \Gamma_{\text{in}}(s) p_0(s)$. Because we disregard initial transients, the probability $p_0(s)$ to find the quantum dot unoccupied at time s is determined as the asymptotic, and hence periodic, solution of the master equation $\dot{p}_0(t) = -[\Gamma_{\text{in}}(t) + \Gamma_{\text{out}}(t)] p_0(t) + \Gamma_{\text{out}}(t)$. This yields, for the residence time, the result p.d.f.¹⁴

$$\rho_1(\tau) = \frac{\int_0^{T_f} ds \Gamma_{\text{out}}(\tau + s | s) P_1(\tau + s | s) \Gamma_{\text{in}}(s) p_0(s)}{\int_0^{T_f} ds \Gamma_{\text{in}}(s) p_0(s)} \quad (5)$$

Because the two tunnelling rates $\Gamma_{\text{in/out}}(t)$ differ in phase but only little in form, the residence time probability density $\rho_0(\tau)$ for the unoccupied (intervals between 'out' and 'in' events) quantum dot is almost identical to that of the occupied quantum dot.

Data availability

The data that support the plots within this paper and other findings of this study are available from the corresponding author upon request.

References

- Bonet, E., Deshmukh, M. M. & Ralph, D. C. Solving rate equations for electron tunneling via discrete quantum states. *Phys. Rev. B* **65**, 045317 (2002).
- Hofmann, A. et al. Measuring the degeneracy of discrete energy levels using a GaAs/AlGaAs quantum dot. *Phys. Rev. Lett.* **117**, 206803 (2017).

In the format provided by the authors and unedited.

Quantum stochastic resonance in an a.c.-driven single-electron quantum dot

Timo Wagner ^{1*}, Peter Talkner², Johannes C. Bayer ¹, Eddy P. Rugeramigabo¹, Peter Hänggi^{2,3}
and Rolf J. Haug ¹

¹Institut für Festkörperphysik, Leibniz Universität Hannover, Hanover, Germany. ²Institut für Physik, Universität Augsburg, Augsburg, Germany.

³Nanosystems Initiative Munich, Munich, Germany. *e-mail: wagner@nano.uni-hannover.de

Supplementary Information for ”Quantum stochastic resonance in an ac-driven single-electron quantum dot”

Timo Wagner,^{1,*} Peter Talkner,² Johannes C. Bayer,¹ Eddy P. Rugeramigabo,¹ Peter Hänggi,^{2,3} and Rolf J. Haug¹

¹*Institut für Festkörperphysik, Leibniz Universität Hannover, D-30167 Hannover, Germany*

²*Institut für Physik, Universität Augsburg, Universitätsstraße 1, D-86135 Augsburg, Germany*

³*Nanosystems Initiative Munich, Schellingstr. 4, D-80799 München, Germany*

(Dated: December 16, 2018)

Counting statistics without drive

Without external drive ($A = 0$) the counting statistic depends on the asymmetry $\alpha = (\Gamma_{in} - \Gamma_{out})/(\Gamma_{in} + \Gamma_{out})$. The tunneling-in rate $\Gamma_{in} = 1/\langle\tau_1\rangle$ and tunneling-out rate $\Gamma_{out} = 1/\langle\tau_0\rangle$ can be determined from the mean residence times $\langle\tau_0\rangle, \langle\tau_1\rangle$. Fig. S1 shows different Fano factors as a function of the asymmetry parameter α . For the total counting statistic $P(\Delta t, n_\Sigma = n_{in} + n_{out})$ the Fano factor F_Σ (red cycles) lies between $1 \leq F_\Sigma \leq 2$ and for the individual counting statistic $P(\Delta t, n_{in/out})$ the Fano factor $F_{in/out}$ (orange diamonds / green crosses) lies between $0.5 \leq F_{in/out} \leq 1$. The different Fano factors have all been determined for a counting interval Δt of 10 ms.

When the rates are symmetric ($\alpha = 0$) the Fano factor F_Σ equals one, because in this special situation the total counting statistics $P(n_{in} + n_{out})$ behaves like a Poissonian process with rate $\Gamma_\Sigma = 2\Gamma_{in/out}$. With growing asymmetry the ‘in’ and ‘out’ events bunch, causing an increase of the Fano factor F_Σ . When the tunneling rates become very asymmetric ($\alpha \approx \pm 1$) two events always occur at the same time, therefore the Fano factor F_Σ must go to 2.0.

The Fano factor $F_{in/out}$ of the individual counting statistic $P(n_{in/out})$ is instead always smaller than 1.0. The black solid line shows the theoretical expected Fano factor $F_{in/out} = \frac{1}{2}(1 + \alpha^2)$ in the zero-frequency limit^{S1,S2}. Due to the Coulomb-blockade two identical events (‘in-in’ or ‘out-out’) can never follow each other directly, which causes always an antibunching of the individual events. The antibunching is maximized when the rates are symmetric ($\alpha = 0$), in that situation the Fano factor becomes 0.5. When the rates are very asymmetric ($\alpha \approx \pm 1$) the counting statistic $P(n_{in/out})$ follows a Poissonian process ($F_{in/out} = 1$) with rate Γ_{in} ($\alpha = 1$) or Γ_{out} ($\alpha = -1$).

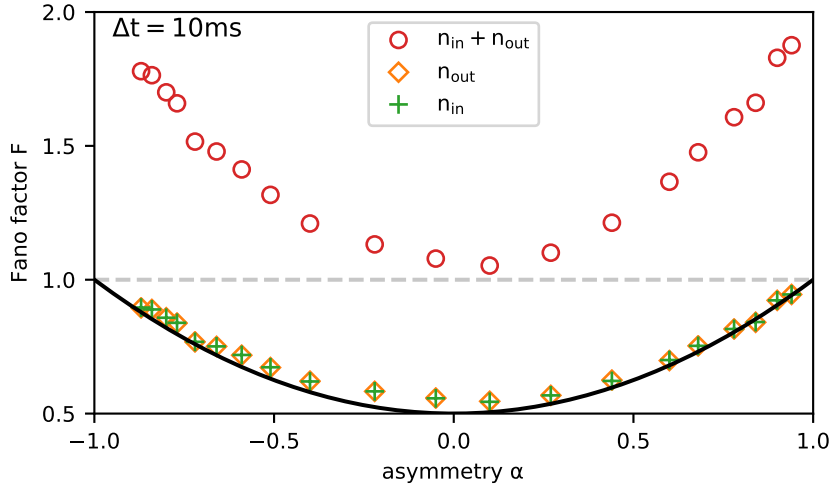


Figure S1: **Fano factor without drive.** The Fano factor without drive ($A = 0$) as a function of the asymmetry $\alpha = (\Gamma_{in} - \Gamma_{out})/(\Gamma_{in} + \Gamma_{out})$. The Fano factor F_Σ (red cycles) of the total counting statistic lies between $1 \leq F_\Sigma \leq 2$. The Fano factor F_Σ (red cycles) lies between $1 \leq F_\Sigma \leq 2$ and the Fano factor $F_{in/out}$ (orange diamonds / green crosses) lies between $0.5 \leq F_{in/out} \leq 1$. The different Fano factors have been determined for a counting interval $\Delta t = 10$ ms. The black solid line is the theoretical expected Fano factor $F_{in/out} = \frac{1}{2}(1 + \alpha^2)$.

Individual 'In' and 'Out' tunneling statistics

Fig.S2a shows the frequency dependent Fano factor $F_{in/out}$ (orange diamonds / green crosses) of the individual counting statistic $P(T_f = 1/f, n_{in/out})$ and the Fano factor F_Σ (red cycles) of the total counting statistics $P(T_f = 1/f, n_\Sigma)$. Fig.S2b shows additionally the corresponding individual mean counts $\langle n_{in/out} \rangle$ as well as the total mean counts $\langle n_\Sigma \rangle := \langle n_{in} + n_{out} \rangle$. The Fano factor $F_{in/out}$ runs through a minimum, which occurs at a slightly slower driving frequency $f = 600$ Hz than the minimum at $f = 800$ Hz in the Fano factor F_Σ . The minimum in $F_{in/out}$ does not fall below 0.5, which makes a clear distinction from the non driven counting statistics (Fig. S1) difficult. This difficulty does not occur for F_Σ , which clearly falls below 1.0.

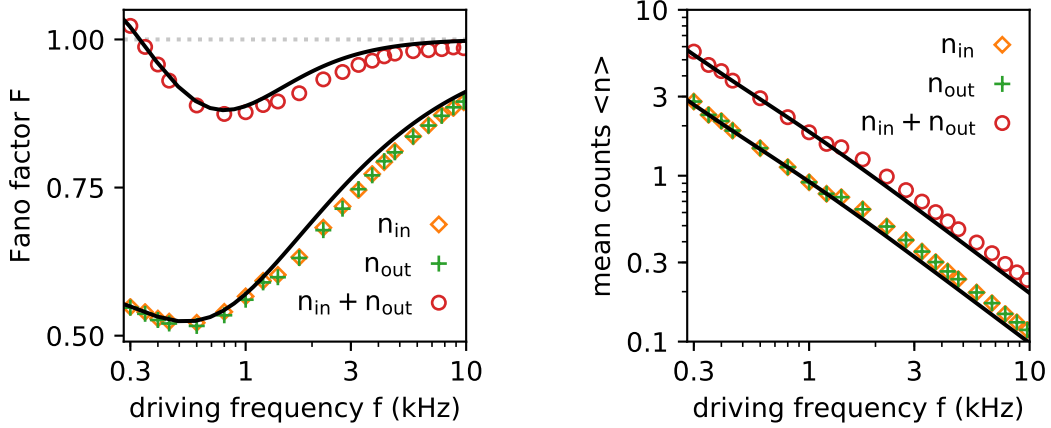


Figure S2: **Frequency dependent counting statistics.** (a) The Fano factor $F_{in/out}$ (orange diamonds / green crosses) of the individual counting statistics and the Fano factor F_Σ (red cycles) for the total counting statistics of a periodically driven QD with driving amplitude $A = 10$ mV. The theoretical expected Fano factors and mean counts (black solid lines) agree nicely with the experimental values. (b) The corresponding individual mean counts $\langle n_{in/out} \rangle$ (orange diamonds / green crosses) and total mean counts $\langle n_\Sigma \rangle := \langle n_{in} + n_{out} \rangle$.

Frequency Locking

Here we discuss the single-electron counting statistics and tunneling rates for a larger driving amplitude $A = 30$ mV than in the main text. Fig. S3a shows the corresponding mean counts $\langle n \rangle$ and Fig. S3b the Fano factor F as a function of the driving frequency f . For this significantly stronger drive a plateau-like feature appears in the mean counts $\langle n \rangle$, corresponding to a locking of the Rice frequency. In the same frequency range the Fano factor F is strongly suppressed below the Poissonian limit ($F_P = 1$), indicating that unwanted random tunneling events are effectively suppressed. The black solid lines in Fig. S3a,b are the theoretical counting statistics, expected from the tunneling rates in Fig. S3c. The rates have been extracted from the detector trace with $f = 1.5$ kHz using Eq. 4 from the main text.

The locking is a consequence of the strong modulation of the tunneling rates. In the first half of a driving period ($0 \leq t < T_F/2$), the in-rate becomes so large that an electron tunnels almost with a probability of one into the QD. At the same time the out-rate is suppressed to the extent that the probability to leave the quantum dot is almost zero. In the second half of a driving period ($T_F/2 \leq t < T_f$) the out-rate is increased to the extent that the ejection of the electron is almost certain. At the same time the in-rate is strongly suppressed that an electron is prevented from tunneling into the dot.

However the electron transfer is still based on the stochastic tunneling process. When the drive becomes too slow the probability of unwanted events increases and if the drive is too fast the probability to miss a tunneling event increases. Therefore the locking is only valid in a certain regime ($\min \{\Gamma_{in/out}(t)\} \ll f \ll \max \{\Gamma_{in/out}(t)\}$), which results from the same time scale matching as SR.

Although the tunneling rates are not harmonic and their forms are quite different, the double driving frequency $2f \approx 3.0$ kHz still is surprisingly close to the tunneling coupling $\Gamma_S = 2.5$ kHz.

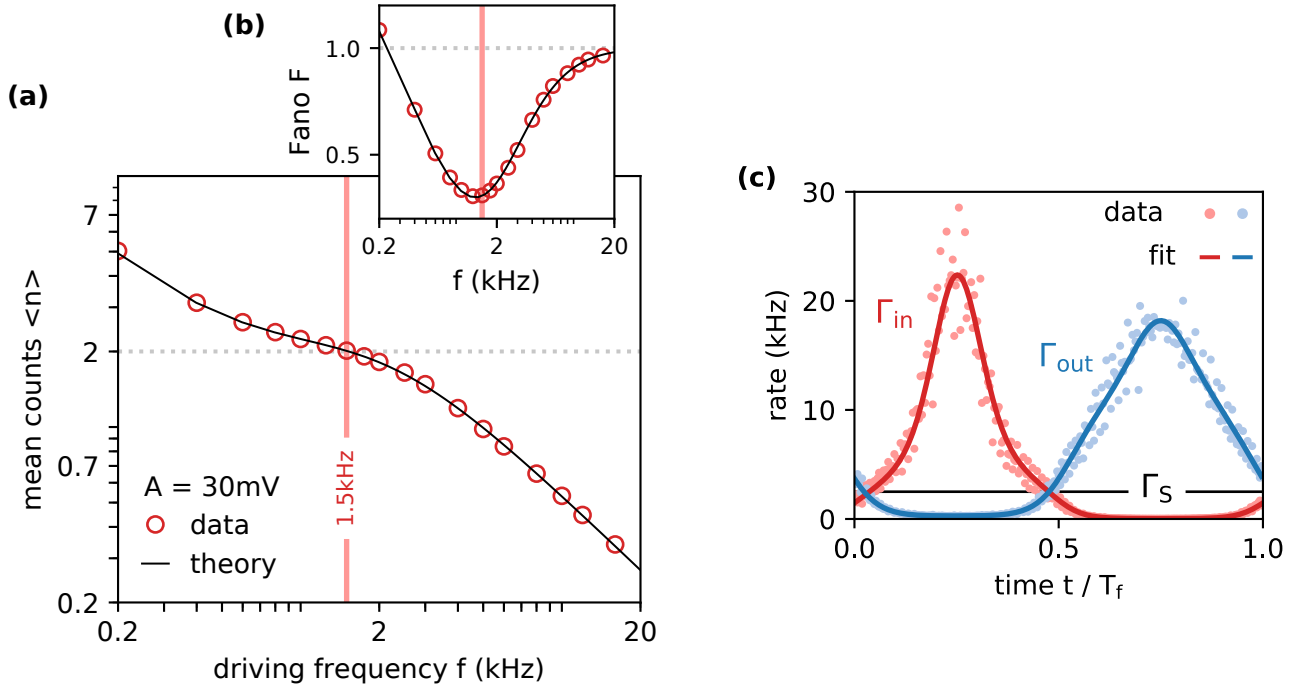


Figure S3: **Frequency locking.** (a) The experimental (red cycles) and theoretical (black line) number of tunneling events per period $\langle n \rangle$ as a function of the driving frequency f . (b) The frequency dependent Fano factor F . (c) Experimentally determined tunneling-in rate $\Gamma_{in}(t)$ (red dots) and tunneling-out rate $\Gamma_{out}(t)$ (blue dots). The rates have been extracted for a drive with $f = 1.5$ kHz and $A = 30$ mV. The fits (solid lines) are based on a Fourier expansion of the logarithm of the rates. The horizontal black line marks the tunnel coupling $\Gamma_S = 2.5$ kHz at symmetry level μ_S .

* Electronic address: wagner@nano.uni-hannover.de

[S1] Bagrets, D. A. & Nazarov, Y. V. Full counting statistics of charge transfer in Coulomb blockade systems. *Phys. Rev. B* **67**, 085316 (2003).

[S2] Gustavsson, S. *et al.* Counting statistics of single-electron transport in a quantum dot. *Phys. Rev. Lett.* **96**, 076605 (2006)

QUANTUM PHYSICS

Noise put to use

Through stochastic resonance, noise-driven fluctuations make an otherwise weak periodic signal accessible. Experiments have now reported quantum stochastic resonance, which arises from intrinsic quantum fluctuations rather than external noise.

Stefan Ludwig

Noise is usually perceived as something negative — just think of electronic noise obscuring signal transmission.

At the same time, random fluctuations induced by noise are an integral and important element of nature, and even life. Under non-equilibrium conditions, they may even become a driving force — as happens for the ratchet mechanism, which turns fluctuations into directed motion¹. Another remarkable noise-driven phenomenon is stochastic resonance², where irregular fluctuations can amplify the effect of an otherwise weak signal. Originally introduced in Earth science to model the recurrence of ice ages³, stochastic resonance has been observed and explored in a broad range of fields, including nonlinear optics, solid-state physics, biology, and even medicine². In most examples, the fluctuations driving stochastic resonance arise from classical sources of noise in the surrounding environment. Now, writing in *Nature Physics*, Timo Wagner and co-authors report the realization of a textbook example of a quantum version of stochastic resonance^{4,5}, where the defining fluctuations are not caused by coupling to a noisy environment; rather, they are an intrinsic property of a quantum two-level system⁶.

The concept of stochastic resonance is illustrated in Fig. 1. It takes place in bistable systems, represented by the double-well potential (Fig. 1a). Stochastic resonance describes the amplification of the effect of a weak signal owing to noise-driving transitions between the system's two fixed points. Of particular interest is the case where the system is exposed to strong noise peaked at a rate that is twice the modulation frequency of the weak periodic signal, as it can lead to synchronization of the noise-driven transitions with a signal that is too weak to drive transitions itself.

The bistable system used in the experiments of Wagner and co-authors is an artificial molecule — a semiconducting lateral double quantum dot. The fixed points of this bistable system correspond to a single electron occupying either the left or the

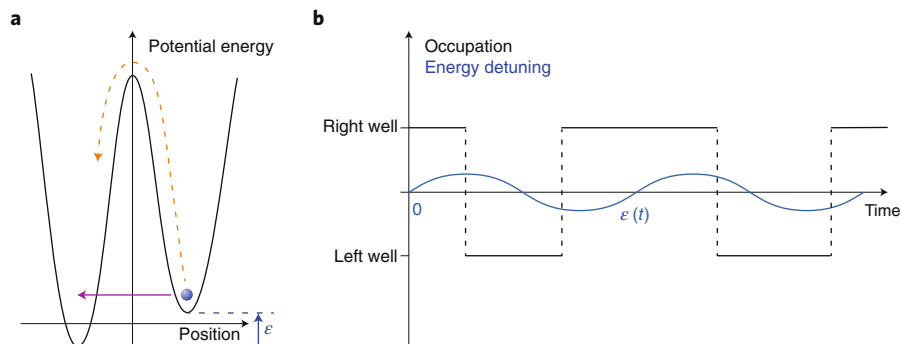


Fig. 1 | Illustration of stochastic resonance. **a**, A bistable system is illustrated as a particle (blue sphere) in a double-well potential. The potential energy of the particle differs by the detuning ϵ between the two wells. The particle oscillates between the two wells with a characteristic rate Γ that gives rise to a steady-state-occupation difference between the two wells depending on ϵ . In the classical limit the oscillation is always caused by energy exchange with the environment (orange dashed arrow), but it can alternatively occur via tunnelling (purple arrow), prevailing the quantum limit. In both cases, the dynamics is probabilistic. **b**, A weak modulation of the detuning, such as $\epsilon(t) = \epsilon_0 \sin(2\pi f_0 t)$, can cause an oscillation of the momentary steady-state occupation, where the details of the system's dynamics depend on the ratio Γ/f_0 . Near the extrema of the modulated $\epsilon(t)$, the energy difference between the wells makes hopping a little easier in one direction and a little harder in the other. A synchronization between tunnelling and modulation requires $\Gamma \sim 2f_0$, essentially because the particle can only tunnel to the right/left well as long as it occupies the left/right well. In the sketch, stochastic resonance is expressed by the tunnelling events happening near the extrema of $\epsilon(t)$. However, given their stochastic nature, the exact time of each tunnelling event still fluctuates.

right dot, illustrated by the two wells of the potential shown in Fig. 1a. An advantage of this nanodevice is its full controllability, which makes it an interesting platform for applications in quantum technologies. The dynamics of the double quantum dot exhibits random fluctuations of the electron hopping between the two dots. The fluctuations might be activated by coupling to external noise or can be restricted to quantum tunnelling through the barrier. In both cases, they can be described by the hopping rate, Γ . The experiment by Wagner and co-authors was realized in a noiseless environment at cryogenic temperatures, where quantum-mechanical tunnelling dominates the dynamics.

To realize stochastic resonance, the authors applied a weak periodic modulation with frequency f_0 of the energy detuning ϵ between the two wells, $\epsilon(t) = \epsilon_0 \sin(2\pi f_0 t)$, of

absolute value much smaller than the height of the potential barrier. In the adiabatic limit, for $f_0 \ll \Gamma$, rapid tunnelling through the barrier guarantees a charge distribution according to the momentary potential shape; the average electron position will oscillate between the two wells in phase with the modulation of ϵ . In the opposite limit, $f_0 \gg \Gamma$, the electron cannot follow the much quicker variations of the local potential, experiencing instead its average value. The most interesting dynamics occurs for $2f_0 \sim \Gamma$, as under this condition the electron typically tunnels twice through the barrier per modulation period. The electron motion then tends to synchronize with the modulation of ϵ , even if the tunnelling dynamics is incoherent. A hand-waving argument for the appearance of synchronization is that it allows the electron to occupy mostly the lower-lying well, minimizing the system energy.

The lateral double quantum dot used by Wagner and co-authors has the advantage of a wide tunability based on the electric field effect of both Γ and ϵ . To realize a perfect example of stochastic resonance, they made use of two additional well-established methods. First, they measured the current through a quantum point contact to detect the charge distribution within the double quantum dot⁷. Second, they combined a relatively small tunnelling rate $\Gamma \sim 1$ MHz with a high (20 MHz) bandwidth current measurement to perform real-time charge detection. In this way, they could detect every single tunnelling event and accumulate a full counting statistics for long enough measurement times⁸.

As a next step, the authors analysed relevant statistical quantities, such as the number of tunnelling events per period, to achieve accurate information about the system dynamics. In particular, the randomness of the tunnelling events is computed via the Fano factor, calculated as the ratio between the variance and the mean value of the tunnelling distribution function. A Fano factor equal to one indicates a completely stochastic Poisson distribution, whereas a value larger than one points to bunching of tunnelling events. Antibunching corresponds to a Fano factor smaller than one, indicating synchronization between subsequent tunnelling events.

Impressively, the authors find a pronounced minimum of this quantity, below one, always centred at $\Gamma = 2f_0$, no matter whether they tune Γ at a fixed modulation frequency f_0 or sweep f_0 for a fixed hopping rate Γ . This is the fundamental characteristic of stochastic resonance.

The role of coherence in the presented experiment remains to be discussed. The dynamics of a quantum system crucially depends on the coherence time — a measure of the speed of the dephasing of the electron's wavefunction. Wagner and co-workers observed stochastic resonance in the incoherent limit, where information on the phase of the electron's wavefunction is lost between successive tunnelling events. It is thanks to decoherence that the stochastic nature of the electron's tunnelling dynamics is indeed maintained. In contrast, the time evolution of the probability function of a fully coherent system is deterministic and, if weakly modulated at $2f_0 \sim \Gamma$, it would show coherent Rabi oscillations of the double-well occupation with a Fano factor much smaller than one, but not necessarily synchronized with the modulation frequency.

With their experiment, Wagner and co-authors have realized a textbook example of stochastic resonance based on quantum tunnelling. An important difference from classical dynamics is

that quantum tunnelling does not require energy exchange with the environment but is an inherent property of the quantum two-state system. This difference allows Wagner and co-authors to report quantum stochastic resonance, a phenomenon that might stimulate new ideas for applications in the incoherent regime, in contrast to fully coherent applications of quantum circuits. An example could be the stabilization of small currents with possible applications for quantum-dot-based current standards. \square

Stefan Ludwig

Paul-Drude-Institut für Festkörperelektronik,
Leibniz-Institut im Forschungsverbund Berlin e. V.,
Berlin, Germany.
e-mail: ludwig@pdi-berlin.de

Published online: 4 February 2019
<https://doi.org/10.1038/s41567-019-0442-7>

References

1. Feynman, R. *The Feynman Lectures on Physics* Vol. I (Basic Books, New York, 2011).
2. Gammaitoni, L. et al. *Rev. Mod. Phys.* **70**, 223–287 (1998).
3. Benzi, R. et al. *J. Phys. A* **14**, L453 (1981).
4. Löfstedt, R. & Coppersmith, S. N. *Phys. Rev. Lett.* **72**, 1947–1950 (1994).
5. Grifoni, M. & Hänggi, P. *Phys. Rev. Lett.* **76**, 1611–1614 (1996).
6. Wagner, T. et al. *Nat. Phys.* <https://doi.org/10.1038/s41567-018-0412-5> (2019).
7. Field, M. et al. *Phys. Rev. Lett.* **70**, 1311–1314 (1993).
8. Gustavsson, S. et al. *Phys. Rev. Lett.* **96**, 076605 (2006).

ACTIVE NEMATICS

Turbulent beginnings

An inspired experimental approach sheds light on the formation of active turbulence in a system of microtubules and molecular motors. The emergent scaling behaviour takes us a step closer to understanding how activity begets turbulence.

Seth Fraden

A comparison between passive and active liquid crystals reveals dramatic differences. A uniformly aligned passive nematic is in its equilibrium state and will remain aligned unless acted upon by an external force. In contrast, a uniformly aligned active nematic is intrinsically unstable; its director spontaneously bends and the fluid begins to flow, driven solely by the consumption of chemical energy. Writing in *Nature Physics*, Berta Martínez-Prat and co-workers have captured the initial instability in a two-dimensional nematic consisting of bundles of microtubules and

their associated kinesin motors deposited on an oil–water interface¹.

The experimental challenge was aligning the active nematic at the beginning of the experiment. In previous studies of this system, the instability, which occurs rapidly, would happen out of sight while the experimenters were loading the samples onto the microscope. To overcome this, the team inserted a straw into the centre of the sample at the oil–water interface, thereby drawing in material and creating radial flows that aligned the microtubules.

The initial state immediately after withdrawing the straw resembled a bicycle wheel with the spokes radiating outward from the hub (Fig. 1a). What followed next was dramatic. First, the aligned microtubule fibres began to undulate as they extended and periodically buckled, leading to a collective instability that resulted in alternating rings of $\pm\frac{1}{2}$ topological defects in the liquid crystal (Fig. 1b). The $+\frac{1}{2}$ defects acted as active quasiparticles that generated flow by propelling themselves forward and reoriented the microtubules into alternating bands of circumferentially